Acta Mech 228, 3543–3559 (2017)
DOI 10.1007/s00707-017-1897-1

ORIGINAL PAPER

Alireza Beheshti

Finite element analysis of plane strain solids in strain-gradient elasticity

Received: 17 November 2016 / Revised: 8 May 2017 / Published online: 28 June 2017

Abstract In the current contribution, plane strain deformation of the strain-gradient solids is addressed using the finite element method. To this end, 4-node quadrilateral elements based on the Hermite shape functions explicitly are developed for predicting the response of two-dimensional solids in small scales. The principle of virtual work is applied to derive the weak form of the equilibrium static equations. In addition, the geometry and variables are interpolated adopting different shape functions resulting in the subparametric elements. For showing the performance and accuracy of the novel elements, some known problems in plane strain elasticity are solved, and there is a comparison between the classical and strain-gradient solutions.

1 Introduction

The displacement field in the classical, static analyses of solids and structures at small scales is larger than the empirical evidences [1]. That is, the experimental results are stiffer than predictions associated with the classical relations. The fact vividly indicates drawbacks of the classical mechanics in fine sizes. In order to solve the problem, Mindlin [2] and Mindlin and Eshel [3] elaborated some gradient theories, Form I, Form II, and Form III, in which the energy density is a function of the strain and the gradient of a kinematic variable. The fact leads to a constitutive equation in which besides the classical material constants there exist some unconventional material parameters. The advantage of the gradient theories may be attributed to these novel material constants. Specifying the new constants is not a straightforward operation experimentally. However, Aifantis [4] proposed the simple, robust strain-gradient model, which is a derivative of Mindlin's Form II [2], and includes one non-classical material constant widely called the length scale parameter.

By deeming the fact that the gradient of kinematic tensors is incorporated in the strain-gradient theory, solving a differential equation is more elaborate in the theory than in classical mechanics. Accordingly, a numerical scheme may be adopted to solve the complex differential equations [5,6], as the analytical solutions are available to us for simple problems only [7–10]. For keen readers, a comprehensive review of both BEM and FEM for static and dynamic gradient elastic problems is presented by Tsinopoulos et al. [11]. In the following two paragraphs, it is aimed at providing some relevant information concerning the finite element method and its application to the gradient theories. The former addresses the C^1-continuous elements for solids, and the latter is concerned with the mixed finite element method in which C^0-continuous elements are developed.

Even though the idea of using C^1-continuous elements is simple in nature, compared with the mixed finite element scheme, developing some elements which are convergent and accurate is complex, as defining the high-order DOF in every node does not guarantee the continuity of variables and their derivates in the element boundaries. As an evidence, the elements developed for the analysis of Kirchhoff–Love plates can be taken into account [12]. Akarapu and Zbib [13] analyzed a crack tip problem adopting a 36-DOF triangular element,

A. Beheshti (✉)
Department of Mechanical Engineering, University of Guilan, Rasht, Iran
E-mail: beheshti.arza@gmail.com

originally elaborated by Dasgupta and Sengupta [14] for plate bending, which is C^1-continuous on the basis of simplified strain-gradient elasticity developed by Aifantis [4]. A C^1 hexahedral element was devised by Papanicolopulos et al. [15] in order to predict the response of three-dimensional solids in small scales. Zervos et al. [16] took advantage of triangular and quadrilateral elements provided by Argyris et al. [17] and Petera and Pittman [18], respectively, for solving boundary value problems in gradient elasticity. It is worthy of note that in addition to [15] Zervos [19] presented some three-dimensional isoparametric elements based on the general Mindlin's theory [2].

By applying the mixed finite element formulation, the need for constructing higher-order elements in the gradient elasticity can be bypassed. However, the scheme has its own complexities. In this area, Shu et al. [20] considered the Fleck–Hutchinson strain gradient theory [21] which is an extension of the original work of Mindlin [2], and by using the mixed finite element method they produced some finite elements for two-dimensional analyses. Amanatidou and Aravas [22] analyzed strain-gradient elasticity problems using mixed finite element formulations. In the work, all three forms of Mindlin's theory [2] were considered, and the performance of C^0-continuous elements was investigated in plane strain problems along with mode-III crack analysis. By adopting the Hu–Washizu principle and consequently the mixed FEM, Imatani et al. [23] analyzed some problems in the two-dimensional strain-gradient elasticity. Askes and Gutiérrez [24] reformulated the gradient elasticity in which finite elements may be constructed by satisfying C^0-continuity only. The finite element method was a tool for Askes et al. [25] to survey the size-dependent behavior of solids. In this work, for producing C^0-continuous elements, the original fourth-order equations of gradient elasticity were divided up into two second-order equations. Following presenting mixed FE formulations analytically [26,27], Markolefas et al. [28] solved some 2D problems in the gradient elasticity.

Besides the conventional finite element method dealt with in detail above, other numerical schemes, such as meshless method, isogeometric analysis, and boundary element method, have been adopted to solve problems in the gradient elasticity. It is not the aim of the current contribution to review associated articles; however, interested researchers are highly recommended to study these works [11,29–32].

In this article, the basis is on the subparametric C^1-continuous quadrilateral elements for the plane strain solid in the strain-gradient medium. Accordingly, the work has nothing in common with the works based on the mixed finite element method mentioned above. For constructing the shape functions, the explicit form of the Hermite polynomials is applied to the FE formulation. It must be emphasized that the elements developed herein are completely novel and somehow very close to the rectangular elements presented by Bogner et al. [33] that two of those are the most accurate elements for an analysis of classical plates. While higher-order quadrilateral elements used by Zervos et al. [16] and Zervos [19] are isoparametric, they consequently need more geometrical data or adopt just Hermite functions implicitly.

As mentioned above, the major focus of this work is producing 4-node quadrilateral elements given the Hermite shape functions for the plane strain analyses of the strain-gradient solids. A review in the literature indicates that the class of elements is novel not only in the gradient mechanics, but also in the classical mechanics. Section 2 that is concerned with basics of the strain-gradient elasticity is followed by Sect. 3 including some data regarding plane strain deformation in the strain-gradient medium. Following the introduction of the principle of virtual work for the current study in Sect. 4, the formulation of the finite element method is presented in Sect. 5. In addition, some numerical examples are solved in Sect. 6. Finally, a conclusion is drawn in Sect. 7.

2 Basics of the strain-gradient theory

Mindlin [2] proposed a model for the deformation of elastic solids in which a so-called micro volume element was embedded in the conventional volume element in order to predict the response of solids in small scales. Furthermore, some assumptions were carried out for simplifying the initially derived model, which may be called elasticity with microstructure. These suppositions lead to three separate models, including Form I, Form II and Form III, for small elastic deformations. Among these forms, Form II in which the gradient of the strain tensor plays a key role is widely used in the literature. In addition, the components of strain tensor $\boldsymbol{\varepsilon}$ and strain-gradient tensor $\boldsymbol{\kappa} = \nabla\boldsymbol{\varepsilon}$ may be given as

$$\varepsilon_{jk} = \varepsilon_{kj} = \frac{1}{2}\left(\frac{\partial u_j}{\partial x_k} + \frac{\partial u_k}{\partial x_j}\right), \tag{1}$$

$$\kappa_{ijk} = \kappa_{ikj} = \frac{\partial \varepsilon_{jk}}{\partial x_i} = \frac{1}{2}\left(\frac{\partial^2 u_j}{\partial x_k \partial x_i} + \frac{\partial^2 u_k}{\partial x_j \partial x_i}\right), \tag{2}$$

Furthermore, the constitutive equations in the strain-gradient theory may be defined as [2,3]

$$\sigma_{ij} = \sigma_{ji} = \frac{\partial W}{\partial \varepsilon_{ij}} = \lambda \varepsilon_{kk}\delta_{ij} + 2\mu\varepsilon_{ij}, \tag{3}$$

$$\tau_{ijk} = \tau_{ikj} = \frac{\partial W}{\partial \kappa_{ijk}} = \frac{1}{2}a_1\left(\delta_{ij}\kappa_{kpp} + 2\delta_{kj}\kappa_{ppi} + \delta_{ik}\kappa_{jpp}\right) + 2a_2\delta_{jk}\kappa_{ipp} + a_3\left(\delta_{ij}\kappa_{ppk} + \delta_{ik}\kappa_{ppj}\right) + 2a_4\kappa_{ijk} + a_5\left(\kappa_{jki} + \kappa_{kji}\right). \tag{4}$$

In the above relations, λ and μ can be called the Lamé's constants. In addition, there exist five non-classical material unknowns, $a_1 - a_5$, in Eq. (4) which may be regarded as the constitutive equation for higher-order quantities. The Aifantis' model [4] for the strain-gradient elasticity may be obtained by supposing that relations $a_1 = a_3 = a_5 = 0$, $a_2 = \frac{1}{2}l^2\lambda$ and $a_4 = l^2\mu$ hold. Furthermore, Lazar and Maugin [34] explained how requiring that the stress–strain symmetry of the elastic energy is also valid for the gradient terms leads to the simple, robust strain-gradient elasticity offered by Aifantis [4]. As may be seen, the effects of the five non-classical parameters are replaced with the parameter l that is called the material length scale constant. It will be shown in the numerical samples that the length scale features prominently in the strain-gradient theory. Accordingly, the double stresses have the following simplified form:

$$\tau_{ijk} = \tau_{ikj} = l^2(\lambda\kappa_{ipp}\delta_{jk} + 2\mu\kappa_{ijk}). \tag{5}$$

3 Plane strain model

In this Section, initially the strain field for the plane strain condition are presented. Subsequently, the stress field is computed using the derived strains together with the constitutive relation presented in the preceding Section.

3.1 Strain components

In the plane strain analyses, it is supposed that there is no displacement along the axis perpendicular to the deformation plane. In the current investigation, the x_1x_2-plane is the plane of interest and the x_3-axis is the restricted axis. The proposed assumption reduces a three-dimensional problem to a plane two-dimensional one. In other words, the equations are based on the coordinates x_1 and x_2. The specified displacement field has practical uses. For the analyses in which the body is long enough in a special direction and tractions have no components along the axis, it is feasible to approximate the solution of a three-dimensional problem by a two-dimensional one. Another practical application of the plane strain problems is the case in which a specimen is totally restricted between two rigid walls constricting the movement of particles in the direction which is normal the walls. Considering all the above-mentioned information, the following displacement field may be proposed for this group of problems [35,36]:

$$u_1 = u_1(x_1, x_2), \quad u_2 = u_2(x_1, x_2), \quad u_3 = 0. \tag{6}$$

As mentioned in the previous Section, in the Form II, both the strain tensor and its gradient are present in the energy-density. Upon inserting Eq. (6) in Eqs. (1) and (2), the following strain–displacement relations may be obtained:

$$\varepsilon_{11} = \frac{\partial u_1}{\partial x_1}, \quad \varepsilon_{22} = \frac{\partial u_2}{\partial x_2}, \quad \varepsilon_{12} = \frac{1}{2}\left(\frac{\partial u_1}{\partial x_2} + \frac{\partial u_2}{\partial x_1}\right), \tag{7}$$

$$\kappa_{111} = \frac{\partial^2 u_1}{\partial x_1^2}, \quad \kappa_{211} = \frac{\partial^2 u_1}{\partial x_1 \partial x_2}, \quad \kappa_{122} = \frac{\partial^2 u_2}{\partial x_1 \partial x_2}, \quad \kappa_{222} = \frac{\partial^2 u_2}{\partial x_2^2},$$

$$\kappa_{112} = \frac{1}{2}\left(\frac{\partial^2 u_1}{\partial x_1 \partial x_2} + \frac{\partial^2 u_2}{\partial x_1^2}\right), \quad \kappa_{212} = \frac{1}{2}\left(\frac{\partial^2 u_1}{\partial x_2^2} + \frac{\partial^2 u_2}{\partial x_1 \partial x_2}\right), \tag{8}$$

with

$$\varepsilon_{33} = \varepsilon_{13} = \varepsilon_{23} = 0, \tag{9}$$

$$\kappa_{i33} = \kappa_{i13} = \kappa_{i23} = \kappa_{311} = \kappa_{322} = \kappa_{312} = 0, \quad i \in \{1, 2, 3\}. \tag{10}$$

3.2 Stress components

In the preceding Subsection, all components of the strain and strain-gradient tensors were computed in the semi-inverse scheme. Now, the focus is on the computation of the stress and double-stress tensors. Accordingly, by deeming Eqs. (3) and (5), the non-zero stresses and double stresses may be expressed as follows:

$$\sigma_{11} = (\lambda + 2\mu)\varepsilon_{11} + \lambda\varepsilon_{22}, \quad \sigma_{22} = \lambda\varepsilon_{11} + (\lambda + 2\mu)\varepsilon_{22}, \quad \sigma_{12} = 2\mu\varepsilon_{12}, \tag{11}$$

$$\begin{aligned} &\tau_{111} = l^2(\lambda + 2\mu)\kappa_{111} + l^2\lambda\kappa_{122}, \quad \tau_{112} = 2l^2\mu\kappa_{112}, \quad \tau_{122} = l^2\lambda\kappa_{111} + l^2(\lambda + 2\mu)\kappa_{122}, \\ &\tau_{211} = l^2\lambda\kappa_{222} + l^2(\lambda + 2\mu)\kappa_{211}, \quad \tau_{212} = 2l^2\mu\kappa_{212}, \quad \tau_{222} = l^2\lambda\kappa_{211} + l^2(\lambda + 2\mu)\kappa_{222}. \end{aligned} \tag{12}$$

It is worthy of note that the above-mentioned relations are constitutive equations for the plane strain deformation in the strain-gradient elasticity.

4 Variational formulation

The principle of virtual work for the Form II of Mindlin's theory in infinitesimal deformation may be expressed as follows [2,3]:

$$\underbrace{\int_V \left(\sigma_{ij}\delta\varepsilon_{ij} + \tau_{ijk}\delta\kappa_{ijk}\right)\mathrm{d}V}_{\delta U} - \underbrace{\left\{\int_V F_k\delta u_k \mathrm{d}V + \int_S \left(\hat{P}_k\delta u_k + \hat{R}_k D\delta u_k\right) dS\right\}}_{\delta W^{\mathrm{ext}}} = 0 \tag{13}$$

where δU and δW^{ext} are variation of the potential energy and the variation of work done by external forces, respectively. In addition, F_k is the body force per unit volume, and $\hat{P}_k$ and $\hat{R}_k$ are the generalized surface tractions [3]. Furthermore, it is supposed that $\hat{R}_k = 0$ on external surfaces in this work.

It should be noted that, in the plane strain problems, some components of stress, double-stress, strain and strain-gradient tensors disappear; hence, the simplified version of the variation of the potential energy may be given by

$$\begin{aligned} \delta U = \int_V &(\sigma_{11}\delta\varepsilon_{11} + \sigma_{22}\delta\varepsilon_{22} + 2\sigma_{12}\delta\varepsilon_{12} \\ &+\tau_{111}\delta\kappa_{111} + \tau_{211}\delta\kappa_{211} + \tau_{122}\delta\kappa_{122} + \tau_{222}\delta\kappa_{222} + 2\tau_{112}\delta\kappa_{112} + 2\tau_{212}\delta\kappa_{212})\mathrm{d}V. \end{aligned} \tag{14}$$

In the finite element method, researchers are interested in a classification of relations in matrix form. The strategy alleviates the process of writing a finite element code considerably. Hence, for the later use, the stress and strain vectors are defined as $\tilde{\boldsymbol{\sigma}} = \{\sigma_{11}, \sigma_{22}, \sigma_{12}, \tau_{111}, \tau_{211}, \tau_{122}, \tau_{222}, \tau_{112}, \tau_{212}\}^{\mathrm{T}}$ and $\tilde{\boldsymbol{\varepsilon}} = \{\varepsilon_{11}, \varepsilon_{22}, 2\varepsilon_{12}, \kappa_{111}, \kappa_{211}, \kappa_{122}, \kappa_{222}, 2\kappa_{112}, 2\kappa_{212}\}^{\mathrm{T}}$, respectively. Additionally, using Eqs. (11) and (12), the following relation between the two vectors is presented:

$$\tilde{\boldsymbol{\sigma}} = \mathbf{D}\tilde{\boldsymbol{\varepsilon}} \tag{15}$$

where non-zero components of the symmetric material matrix $\mathbf{D}$ are as below:

$$\begin{aligned} &D_{11} = D_{22} = \lambda + 2\mu, \quad D_{12} = \lambda, \quad D_{33} = \mu, \quad D_{44} = l^2(\lambda + 2\mu), \quad D_{46} = l^2\lambda, \\ &D_{55} = l^2(\lambda + 2\mu), \quad D_{57} = l^2\lambda, \quad D_{66} = l^2(\lambda + 2\mu), \\ &D_{77} = l^2(\lambda + 2\mu), \quad D_{88} = l^2\mu, \quad D_{99} = l^2\mu. \end{aligned} \tag{16}$$

5 Finite element formulation

In the finite element method, the body is divided into some smaller parts called elements. Within every element, some nodes may be distributed in order to approximate not only the variables but also the geometry of the domain. It is worth noting that in the subparametric concept applied to the current study the variables and geometry are interpolated using different shape functions. That is, in the subparametric elements, the order of shape functions applied to the geometry is lower than those used to interpolate the variables [37]. The finite

element approximation for the typical domain of a plane strain problem Ω is defined by Ω^h. Additionally, considering Ω_e as a typical element, the approximated region may be expressed as $\Omega^h = \mathbf{A}_{e=1}^{n_e} \Omega_e$.

In the gradient theory, higher-order derivates of the displacement field are present in the equations. Accordingly, in order to produce conforming elements, higher-order derivates of variables must be defined as degrees of freedom. In this contribution, the novel conforming finite elements fulfill the C^1-continuity on the domain, while the geometry is approximated according to the classical plane problems. It is worthy of note that both elements are classified as the subparametric elements, as the order of shape functions for interpolating the geometry is lower than that of the variables. The plane strain elements developed herein have both 4 nodes, but 6 DoF and 12 DoF per node, respectively. The former is abbreviated to PS6, and the latter is shortened to PS12. It must be mentioned that the PS12 is more accurate than PS6. The reason is explained in the next Sections.

5.1 Transformation of derivatives of a function

It is essential to transform derivatives of a function with respect to x_1 and x_2 coordinates to the derivatives with respect to the natural coordinates, i.e., ξ and η. The procedure is a fundamental step for producing the plane strain elements. Using the chain rule and conducting some straightforward mathematical operations, the following relation may be extracted for the transformation:

$$\begin{Bmatrix} \frac{\partial f}{\partial \xi} \\ \frac{\partial f}{\partial \eta} \\ \frac{\partial^2 f}{\partial \xi^2} \\ \frac{\partial^2 f}{\partial \eta^2} \\ \frac{\partial^2 f}{\partial \xi \partial \eta} \end{Bmatrix} = \underbrace{\begin{bmatrix} \frac{\partial x_1}{\partial \xi} & \frac{\partial x_2}{\partial \xi} & 0 & 0 & 0 \\ \frac{\partial x_1}{\partial \eta} & \frac{\partial x_2}{\partial \eta} & 0 & 0 & 0 \\ \frac{\partial^2 x_1}{\partial \xi^2} & \frac{\partial^2 x_2}{\partial \xi^2} & \left(\frac{\partial x_1}{\partial \xi}\right)^2 & \left(\frac{\partial x_2}{\partial \xi}\right)^2 & 2\frac{\partial x_1}{\partial \xi}\frac{\partial x_2}{\partial \xi} \\ \frac{\partial^2 x_1}{\partial \eta^2} & \frac{\partial^2 x_2}{\partial \eta^2} & \left(\frac{\partial x_1}{\partial \eta}\right)^2 & \left(\frac{\partial x_2}{\partial \eta}\right)^2 & 2\frac{\partial x_1}{\partial \eta}\frac{\partial x_2}{\partial \eta} \\ \frac{\partial^2 x_1}{\partial \xi \partial \eta} & \frac{\partial^2 x_2}{\partial \xi \partial \eta} & \frac{\partial x_1}{\partial \xi}\frac{\partial x_1}{\partial \eta} & \frac{\partial x_2}{\partial \xi}\frac{\partial x_2}{\partial \eta} & \frac{\partial x_1}{\partial \xi}\frac{\partial x_2}{\partial \eta} + \frac{\partial x_1}{\partial \eta}\frac{\partial x_2}{\partial \xi} \end{bmatrix}}_{\tilde{\mathbf{J}}} \begin{Bmatrix} \frac{\partial f}{\partial x_1} \\ \frac{\partial f}{\partial x_2} \\ \frac{\partial^2 f}{\partial x_1^2} \\ \frac{\partial^2 f}{\partial x_2^2} \\ \frac{\partial^2 f}{\partial x_1 \partial x_2} \end{Bmatrix} \tag{17}$$

where f is an arbitrary function and $\tilde{\mathbf{J}}$ is the transformation matrix. Reversely, the inverse of the matrix $\tilde{\mathbf{J}}$ shown by $\hat{\mathbf{J}}$ may be used to find derivatives of the function f with respect to x_1 and x_2 coordinates when initially derivatives with respect to ξ and η are available. These transformations matter enormously in the current finite element formulation.

5.2 Finite element formulation with PS6

In this Subsection, some information concerning the formulation of the 4-node quadrilateral element with 6 degrees of freedom per every node is presented. The technique relatively eases the construction of elements; however, the convergence of elements must be examined in order to achieve more reliable results [38]. Accordingly, the following vector may be considered as nodal displacement in every node:

$$\hat{\mathbf{d}}_I = \left\{ u_1|_I, \frac{\partial u_1}{\partial x_1}|_I, \frac{\partial u_1}{\partial x_2}|_I, u_2|_I, \frac{\partial u_2}{\partial x_1}|_I, \frac{\partial u_2}{\partial x_2}|_I \right\}^{\mathrm{T}}. \tag{18}$$

Here, the geometry of an element may be approximated by

$$\mathbf{x}_e = \sum_{I=1}^{4} N_I(\xi, \eta)\mathbf{x}_I \tag{19}$$

where $\mathbf{x}_I$ are the nodal coordinate vectors.

For interpolating the variables, i.e., displacements, different interpolation functions from the geometry are chosen, since derivates appear in the nodal displacement. The strategy applied herein is so close to the scheme which is used for producing beam elements based on the Euler–Bernoulli model at small deformations. In Euler–Bernoulli beam finite elements, different shape functions are considered for geometry and variables.

Additionally, in the strain-gradient context, the Timoshenko beam model has also the same trend as conducted in [39] for producing conforming beam elements. Since defining shape functions with respect to the coordinates in the parent element is so beneficial, initially higher-order derivatives are deemed with respect to the parent coordinates, and then by taking the advantage of Eq. (17) all the derivatives are converted to the original space. To this end, we have

$$S|_e = \sum_{I=1}^{4} \left\{ H_I^{(3)}(\xi,\eta) S|_I + \bar{H}_I^{(3)}(\xi,\eta) \frac{\partial S}{\partial \xi}|_I + \tilde{H}_I^{(3)}(\xi,\eta) \frac{\partial S}{\partial \eta}|_I \right\} \tag{20}$$

where S plays the role of u_1, u_2, δu_1, and δu_2.

Subsequently, Eq. (17) can be used to define the degrees of freedom with respect to the x_1 and x_2 coordinates. By applying the transformation, the following form of the field S may be achieved:

$$S|_e = \sum_{I=1}^{4} \left\{ T_I^{(3)}(\xi,\eta) S|_I + \bar{T}_I^{(3)}(\xi,\eta) \frac{\partial S}{\partial x_1}|_I + \tilde{T}_I^{(3)}(\xi,\eta) \frac{\partial S}{\partial x_2}|_I \right\} \tag{21}$$

with

$$T_I^{(3)}(\xi,\eta) = H_I^{(3)}(\xi,\eta), \tag{22}$$

$$\bar{T}_I^{(3)}(\xi,\eta) = \tilde{J}_{11}|_I \bar{H}_I^{(3)}(\xi,\eta) + \tilde{J}_{21}|_I \tilde{H}_I^{(3)}(\xi,\eta), \tag{23}$$

$$\tilde{T}_I^{(3)}(\xi,\eta) = \tilde{J}_{12}|_I \bar{H}_I^{(3)}(\xi,\eta) + \tilde{J}_{22}|_I \tilde{H}_I^{(3)}(\xi,\eta). \tag{24}$$

After defining the field in the finite element method, the focus is on the stiffness matrix and the external force vector. Upon inserting the approximated displacement fields into Eqs. (7) and (8), and subsequently using the chain rule, i.e., Eq. (17), a finite element approximation of the strain vector may be arranged in the following form:

$$\tilde{\boldsymbol{\varepsilon}}_e = \mathbf{A} \left\{ \frac{\partial u_1|_e}{\partial \xi}, \frac{\partial u_1|_e}{\partial \eta}, \frac{\partial^2 u_1|_e}{\partial \xi^2}, \frac{\partial^2 u_1|_e}{\partial \eta^2}, \frac{\partial^2 u_1|_e}{\partial \xi \partial \eta}, \frac{\partial u_2|_e}{\partial \xi}, \frac{\partial u_2|_e}{\partial \eta}, \frac{\partial^2 u_2|_e}{\partial \xi^2}, \frac{\partial^2 u_2|_e}{\partial \eta^2}, \frac{\partial^2 u_2|_e}{\partial \xi \partial \eta} \right\}^{\mathrm{T}} \tag{25}$$

with

$$\mathbf{A} = \begin{bmatrix} \hat{\mathbf{r}}_1^{\mathrm{T}} & \mathbf{0}^{\mathrm{T}} & \hat{\mathbf{r}}_2^{\mathrm{T}} & \hat{\mathbf{r}}_3^{\mathrm{T}} & \hat{\mathbf{r}}_5^{\mathrm{T}} & \mathbf{0}^{\mathrm{T}} & \mathbf{0}^{\mathrm{T}} & \hat{\mathbf{r}}_5^{\mathrm{T}} & \hat{\mathbf{r}}_4^{\mathrm{T}} \\ \mathbf{0}^{\mathrm{T}} & \hat{\mathbf{r}}_2^{\mathrm{T}} & \hat{\mathbf{r}}_1^{\mathrm{T}} & \mathbf{0}^{\mathrm{T}} & \mathbf{0}^{\mathrm{T}} & \hat{\mathbf{r}}_5^{\mathrm{T}} & \hat{\mathbf{r}}_4^{\mathrm{T}} & \hat{\mathbf{r}}_3^{\mathrm{T}} & \hat{\mathbf{r}}_5^{\mathrm{T}} \end{bmatrix}^{\mathrm{T}} \tag{26}$$

where $\hat{\mathbf{r}}_1$, $\hat{\mathbf{r}}_2$, $\hat{\mathbf{r}}_3$, $\hat{\mathbf{r}}_4$, and $\hat{\mathbf{r}}_5$ are the first to the last rows of the matrix $\hat{\mathbf{J}}$, respectively. Furthermore, the second term in the right-hand side of Eq. (25) may be given as

$$\left\{ \frac{\partial u_1|_e}{\partial \xi}, \frac{\partial u_1|_e}{\partial \eta}, \frac{\partial^2 u_1|_e}{\partial \xi^2}, \frac{\partial^2 u_1|_e}{\partial \eta^2}, \frac{\partial^2 u_1|_e}{\partial \xi \partial \eta}, \frac{\partial u_2|_e}{\partial \xi}, \frac{\partial u_2|_e}{\partial \eta}, \frac{\partial^2 u_2|_e}{\partial \xi^2}, \frac{\partial^2 u_2|_e}{\partial \eta^2}, \frac{\partial^2 u_2|_e}{\partial \xi \partial \eta} \right\}^{\mathrm{T}} = \mathbf{G}\mathbf{d}_e \tag{27}$$

with

$$\mathbf{d}_e = \left\{ \hat{\mathbf{d}}_1^{\mathrm{T}}, \hat{\mathbf{d}}_2^{\mathrm{T}}, \hat{\mathbf{d}}_3^{\mathrm{T}}, \hat{\mathbf{d}}_4^{\mathrm{T}} \right\}^{\mathrm{T}} \tag{28}$$

where $\mathbf{d}_e$ denotes the element displacement vector.

Upon combining Eqs. (25) and (27), the approximated strain vector of an element may be expressed as

$$\tilde{\boldsymbol{\varepsilon}}_e = \mathbf{B}\mathbf{d}_e, \quad \text{with} \quad \mathbf{B} = \mathbf{A}\mathbf{G}. \tag{29}$$

Additionally, by inserting Eq. (29) into Eq. (15), the element stress vector may be expressed by

$$\tilde{\boldsymbol{\sigma}}_e = \mathbf{D}\mathbf{B}\mathbf{d}_e. \tag{30}$$

It is worthy of note that in the variational formulation the variation of the strain tensor appears in the equations; hence, the same procedure may be carried out in order to produce the final variational displacement vector for each node or element. Since the procedure is repetitious, the detailed explorations are not presented for the

variational forms. Simply, those may be achieved by adding the variation symbol before kinematical quantities. Finally, the element variational strain vector is as below:

$$\delta\tilde{\boldsymbol{\varepsilon}}_e = \mathbf{B}\delta\mathbf{d}_e. \tag{31}$$

After preparing the introductory information regarding the various fields on an element, it is time to focus on the variation of the potential energy. Since the depth of the body is constant in the plane strain analysis and there is no dependence on the longitudinal axis, one may plainly replace the volume element with the surface element in the integrals. Thus, Eq. (14) may be written in the following form using the finite element discretization:

$$\delta U = \mathbf{A}_{e=1}^{n_e}\delta\mathbf{d}_e^T\mathbf{k}_e\mathbf{d}_e = \delta\mathbf{d}^{\mathrm{T}}\mathbf{K}\mathbf{d} \quad \text{with} \quad \mathbf{k}_e = \int_{\Omega_e}\mathbf{B}^{\mathrm{T}}\mathbf{D}\mathbf{B}\mathrm{d}\Omega \tag{32}$$

where $\mathbf{d}$ and $\mathbf{K}$ are the global displacement vector and global stiffness matrix, respectively.

Let us focus on the variation of the work done by external forces in the absence of the body forces. By defining the external force vector in each element $\mathbf{f}_e^{\mathrm{ext}}$ and using the last integral in Eq. (13), the following relation is obtained:

$$\delta W^{\mathrm{ext}} = \mathbf{A}_{e=1}^{n_e}\delta\mathbf{d}_e^T\mathbf{f}_e = \delta\mathbf{d}^{\mathrm{T}}\mathbf{F}. \tag{33}$$

In the above term, $\mathbf{F}$ stands for the global load vector.

Finally, considering Eqs. (13), (32), and (33), the following linear algebraic equations can be derived:

$$\mathbf{K}\mathbf{d} = \mathbf{F}. \tag{34}$$

Solving Eq. (34) after applying the boundary conditions leads to the result of the problem.

5.2.1 Shape functions for PS6

In the previous Section, there is no data regarding the precise form of the shape functions for the geometry and variables. For the interpolation of the geometry, the same shape functions as the classical plane strain problem which are the Lagrange shape functions for a 4-node element may be applied. Those read [40]:

$$N_I(\xi,\eta) = \frac{1}{4}(1+\xi_I\xi)(1+\eta_I\eta), \quad I \in \{1,2,3,4\} \tag{35}$$

with

$$\{\xi_1,\xi_2,\xi_3,\xi_4\} = \{-1,1,1,-1\}, \quad \{\eta_1,\eta_2,\eta_3,\eta_4\} = \{-1,-1,1,1\} \tag{36}$$

where the subscript I refers to the node number, see Fig. 1.

The challenging phase is finding the shape functions for variables. The prominent step in specifying the shape functions which are two-variable is to suppose that those are made from the multiplication of one-variable functions of ξ or η. The third-order Hermite polynomial of one variable can be used for constructing final shape functions. Additionally, unknowns of the Hermite functions can be found by applying the following conditions:

$$\underline{H}_{2I-1}^{(3)}(\xi_J) = \delta_{IJ}, \quad \frac{\mathrm{d}\underline{H}_{2I}^{(3)}(\xi_J)}{\mathrm{d}\xi} = \delta_{IJ}. \tag{37}$$

In the above relation, δ_{IJ} is the Kronecker delta, and I and J take the values 1 and 2. In addition, the relations $\xi_1 = -1$ and $\xi_2 = 1$ hold.

Accordingly, the final forms of the third-degree Hermite polynomials are

$$\begin{cases} \underline{H}_1^{(3)}(\xi) = \frac{1}{4}(2-3\xi+\xi^3),\ \underline{H}_2^{(3)}(\xi) = \frac{1}{4}(1-\xi-\xi^2+\xi^3) \\ \underline{H}_3^{(3)}(\xi) = \frac{1}{4}(2+3\xi-\xi^3),\ \underline{H}_4^{(3)}(\xi) = \frac{1}{4}(-1-\xi+\xi^2+\xi^3). \end{cases} \tag{38}$$

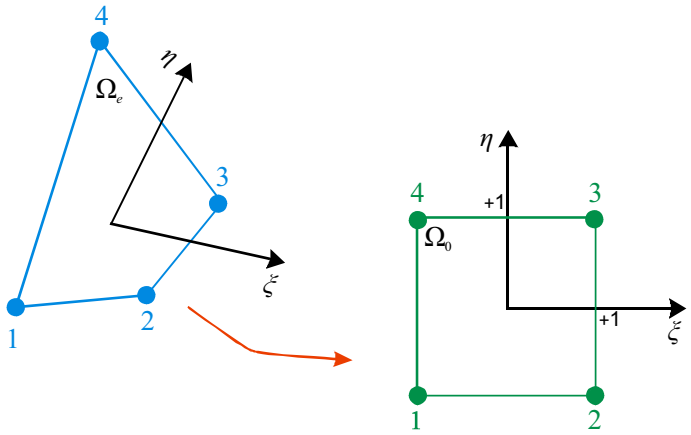

Fig. 1 A typical map from the physical element to the parent element

Subsequently, by deeming similar conditions as presented in Eq. (37), the following newly developed shape functions may be presented for 4-node elements with 6 degrees of freedom per node:

$$\begin{cases} H_I^{(3)} = \underline{H}_r^{(3)}(\xi)\underline{H}_s^{(3)}(\eta), \quad \bar{H}_I^{(3)} = \underline{H}_{r+1}^{(3)}(\xi)\underline{H}_s^{(3)}(\eta), \quad \tilde{H}_I^{(3)} = \underline{H}_r^{(3)}(\xi)\underline{H}_{s+1}^{(3)}(\eta), \\ \{I, r, s\} \in \{\{1,1,1\},\{2,3,1\},\{3,3,3\},\{4,1,3\}\}. \end{cases} \tag{39}$$

Expanding the above polynomials reveals that the displacement field in Eqs. (20) and (21) does not satisfy a special mode. Accordingly, the result of the element, PS6, is not totally accurate [33], say three per cent error.

Another important matrix for 4-node elements is **G** expressed in Eq. (27). This matrix has the following form:

$$\mathbf{G} = \begin{bmatrix} \mathbf{T}_1^A & \mathbf{0} & \mathbf{T}_2^A & \mathbf{0} & \mathbf{T}_3^A & \mathbf{0} & \mathbf{T}_4^A & \mathbf{0} \\ \mathbf{0} & \mathbf{T}_1^A & \mathbf{0} & \mathbf{T}_2^A & \mathbf{0} & \mathbf{T}_3^A & \mathbf{0} & \mathbf{T}_4^A \end{bmatrix} \tag{40}$$

with

$$\mathbf{T}_I^A = \left\{ \frac{\partial \overline{\overline{\mathbf{T}}}_I^T}{\partial \xi}, \frac{\partial \overline{\overline{\mathbf{T}}}_I^T}{\partial \eta}, \frac{\partial^2 \overline{\overline{\mathbf{T}}}_I^T}{\partial \xi^2}, \frac{\partial^2 \overline{\overline{\mathbf{T}}}_I^T}{\partial \eta^2}, \frac{\partial^2 \overline{\overline{\mathbf{T}}}_I^T}{\partial \xi \partial \eta} \right\}^{\mathrm{T}}, \quad \overline{\overline{\mathbf{T}}}_I = \left\{ T_I^{(3)}, \bar{T}_I^{(3)}, \tilde{T}_I^{(3)} \right\}^{\mathrm{T}}. \tag{41}$$

The above information can be used to derive the global stiffness matrix and the force vector.

5.3 Finite element formulation with PS12

In the strain-gradient theory, due to the existence of the gradient of the strain tensor in the equations, one must consider the first and the second derivatives of displacements with respect to the in-plane Cartesian coordinates, i.e., x_1 and x_2, in order to fulfill continuity. It is a critical phase for producing compatible elements. Accordingly, the following vector must be considered as nodal displacement in the finite element method:

$$\hat{\mathbf{d}}_I = \left\{ u_1|_I, \frac{\partial u_1}{\partial x_1}|_I, \frac{\partial u_1}{\partial x_2}|_I, \frac{\partial^2 u_1}{\partial x_1^2}|_I, \frac{\partial^2 u_1}{\partial x_2^2}|_I, \frac{\partial^2 u_1}{\partial x_1 \partial x_2}|_I, u_2|_I, \frac{\partial u_2}{\partial x_1}|_I, \frac{\partial u_2}{\partial x_2}|_I, \frac{\partial^2 u_2}{\partial x_1^2}|_I, \frac{\partial^2 u_2}{\partial x_2^2}|_I, \frac{\partial^2 u_2}{\partial x_1 \partial x_2}|_I \right\}^{\mathrm{T}}. \tag{42}$$

Deem S to be a variable, for instance, the vertical displacement or its variation, for an element. It is approximated by

$$\begin{aligned} S|_e = \sum_{I=1}^{4} \Big\{ & H_I^{(5)}(\xi,\eta) S|_I + \bar{H}_I^{(5)}(\xi,\eta) \frac{\partial S}{\partial \xi}|_I + \hat{H}_I^{(5)}(\xi,\eta) \frac{\partial S}{\partial \eta}|_I + \tilde{H}_I^{(5)}(\xi,\eta) \frac{\partial^2 S}{\partial \xi^2}|_I \\ & + \breve{H}_I^{(5)}(\xi,\eta) \frac{\partial^2 S}{\partial \eta^2}|_I + \widehat{H}_I^{(5)}(\xi,\eta) \frac{\partial^2 S}{\partial \xi \partial \eta}|_I \Big\}. \end{aligned} \tag{43}$$

Subsequently, Eq. (17) can be used to define the derivatives available above with respect to the x_1 and x_2 coordinates. By applying the transformation and some arrangements, the following form of the field S may be achieved:

$$S|_e = \sum_{I=1}^{4} \left\{ T_I^{(5)} S|_I + \bar{T}_I^{(5)} \frac{\partial S}{\partial x_1}|_I + \hat{T}_I^{(5)} \frac{\partial S}{\partial x_2}|_I + \tilde{T}_I^{(5)} \frac{\partial^2 S}{\partial x_1^2}|_I + \breve{T}_I^{(5)} \frac{\partial^2 S}{\partial x_2^2}|_I + \widehat{T}_I^{(5)} \frac{\partial^2 S}{\partial x_1 \partial x_2}|_I \right\} \tag{44}$$

with

$$T_I^{(5)} = H_I^{(5)}(\xi, \eta), \tag{45}$$

$$\bar{T}_I^{(5)} = \tilde{J}_{11}|_I \bar{H}_I^{(5)}(\xi, \eta) + \tilde{J}_{21}|_I \hat{H}_I^{(5)}(\xi, \eta) + \tilde{J}_{31}|_I \tilde{H}_I^{(5)}(\xi, \eta) + \tilde{J}_{41}|_I \breve{H}_I^{(5)}(\xi, \eta) + \tilde{J}_{51}|_I \widehat{H}_I^{(5)}(\xi, \eta), \tag{46}$$

$$\hat{T}_I^{(5)} = \tilde{J}_{12}|_I \bar{H}_I^{(5)}(\xi, \eta) + \tilde{J}_{22}|_I \hat{H}_I^{(5)}(\xi, \eta) + \tilde{J}_{32}|_I \tilde{H}_I^{(5)}(\xi, \eta) + \tilde{J}_{42}|_I \breve{H}_I^{(5)}(\xi, \eta) + \tilde{J}_{52}|_I \widehat{H}_I^{(5)}(\xi, \eta), \tag{47}$$

$$\tilde{T}_I^{(5)} = \tilde{J}_{33}|_I \tilde{H}_I^{(5)}(\xi, \eta) + \tilde{J}_{43}|_I \breve{H}_I^{(5)}(\xi, \eta) + \tilde{J}_{53}|_I \widehat{H}_I^{(5)}(\xi, \eta), \tag{48}$$

$$\breve{T}_I^{(5)} = \tilde{J}_{34}|_I \tilde{H}_I^{(5)}(\xi, \eta) + \tilde{J}_{44}|_I \breve{H}_I^{(5)}(\xi, \eta) + \tilde{J}_{54}|_I \widehat{H}_I^{(5)}(\xi, \eta), \tag{49}$$

$$\widehat{T}_I^{(5)} = \tilde{J}_{35}|_I \tilde{H}_I^{(5)}(\xi, \eta) + \tilde{J}_{45}|_I \breve{H}_I^{(5)}(\xi, \eta) + \tilde{J}_{55}|_I \widehat{H}_I^{(5)}(\xi, \eta). \tag{50}$$

With the knowledge of the approximated field for the 12-DoF quadrilateral element developed in this Section, the same procedures conducted for the PS6 should be followed in order to obtain the global stiffness matrix and the external force, i.e., Eqs. (25)–(34).

5.3.1 Shape functions for PS12

Herein, the same shape functions as the 6-DoF one are used to interpolate geometric properties, i.e., Eq. (35). To specify shape functions for this element based on the Hermite polynomials, similar to the PS6, shape functions presented in Eq. (43) must be decomposed into two one-variable fifth-order Hermite polynomials. To this end, it is essential to investigate functions satisfying the following conditions:

$$\underline{H}_{3I-2}^{(5)}(\xi_J) = \delta_{IJ}, \quad \frac{\mathrm{d}\underline{H}_{3I-1}^{(5)}(\xi_J)}{\mathrm{d}\xi} = \delta_{IJ}, \quad \frac{\mathrm{d}^2\underline{H}_{3I}^{(5)}(\xi_J)}{\mathrm{d}\xi^2} = \delta_{IJ}. \tag{51}$$

Similar to the previous case, i.e., Eq. (37), I and J must be chosen from the set $\{1, 2\}$ and $\xi_1 = -1$ and $\xi_2 = 1$.

By applying the above-mentioned conditions to the fifth-order Hermite polynomials, we have

$$\begin{cases} \underline{H}_1^{(5)} = \frac{1}{16}(8 - 15\xi + 10\xi^3 - 3\xi^5), \\ \underline{H}_2^{(5)} = \frac{1}{16}(5 - 7\xi - 6\xi^2 + 10\xi^3 + \xi^4 - 3\xi^5), \\ \underline{H}_3^{(5)} = \frac{1}{16}(1 - \xi - 2\xi^2 + 2\xi^3 + \xi^4 - \xi^5), \\ \underline{H}_4^{(5)} = \frac{1}{16}(8 + 15\xi - 10\xi^3 + 3\xi^5), \\ \underline{H}_5^{(5)} = \frac{1}{16}(-5 - 7\xi + 6\xi^2 + 10\xi^3 - \xi^4 - 3\xi^5), \\ \underline{H}_6^{(5)} = \frac{1}{16}(1 + \xi - 2\xi^2 - 2\xi^3 + \xi^4 + \xi^5). \end{cases} \tag{52}$$

The above functions may be used to construct shape functions provided in Eq. (43).

Similar to the scheme applied for the 4-node element with six degrees of freedom, the shape functions for interpolation of the variables may be given as

$$\begin{cases} H_I^{(5)} = \underline{H}_r^{(5)}(\xi)\underline{H}_s^{(5)}(\eta), \quad \bar{H}_I^{(5)} = \underline{H}_{r+1}^{(5)}(\xi)\underline{H}_s^{(5)}(\eta), \quad \hat{H}_I^{(5)} = \underline{H}_r^{(5)}(\xi)\underline{H}_{s+1}^{(5)}(\eta), \\ \tilde{H}_I^{(5)} = \underline{H}_{r+2}^{(5)}(\xi)\underline{H}_s^{(5)}(\eta), \quad \breve{H}_I^{(5)} = \underline{H}_r^{(5)}(\xi)\underline{H}_{s+2}^{(5)}(\eta), \quad \widehat{H}_I^{(5)} = \underline{H}_{r+1}^{(5)}(\xi)\underline{H}_{s+1}^{(5)}(\eta), \\ \{I, r, s\} \in \{\{1,1,1\},\{2,4,1\},\{3,4,4\},\{4,1,4\}\}. \end{cases} \tag{53}$$

For extracting the above relations, the same idea used in Eq. (51) needs to be applied. That is to say, the two-variable shape functions may be chosen by considering Eq. (43) along with the fulfillment of each DoF at nodes. The point which must be taken into account here is that the displacement field based on the above functions includes suitable terms for approximating the variables. That is to say, the displacement field meets the special mode proposed by Bogner et al. [33] for the deformation of rectangular plates. Consequently, PS12 provides us with the accurate results.

Now, it is feasible to specify the precise form of the approximated variables based on Eq. (44). Furthermore, differentiation of Eq. (44) with respect to the parent coordinates, i.e., ξ and η, enables one to compute the matrix $\mathbf{G}$ firstly built in Eq. (27) for the 12-DoF element. It is

$$\mathbf{G} = \begin{bmatrix} \mathbf{T}_1^B & \mathbf{0} & \mathbf{T}_2^B & \mathbf{0} & \mathbf{T}_3^B & \mathbf{0} & \mathbf{T}_4^B & \mathbf{0} \\ \mathbf{0} & \mathbf{T}_1^B & \mathbf{0} & \mathbf{T}_2^B & \mathbf{0} & \mathbf{T}_3^B & \mathbf{0} & \mathbf{T}_4^B \end{bmatrix} \tag{54}$$

with

$$\begin{cases} \mathbf{T}_I^B = \{\dfrac{\partial \widehat{\mathbf{T}}_I^T}{\partial \xi}, \dfrac{\partial \widehat{\mathbf{T}}_I^T}{\partial \eta}, \dfrac{\partial^2 \widehat{\mathbf{T}}_I^T}{\partial \xi^2}, \dfrac{\partial^2 \widehat{\mathbf{T}}_I^T}{\partial \eta^2}, \dfrac{\partial^2 \widehat{\mathbf{T}}_I^T}{\partial \xi \partial \eta}\}^T \\ \widehat{\mathbf{T}}_I = \{T_I^{(5)}, \bar{T}_I^{(5)}, \hat{T}_I^{(5)}, \tilde{T}_I^{(5)}, \breve{T}_I^{(5)}, \widehat{T}_I^{(5)}\}^T. \end{cases} \tag{55}$$

Finally, all details about the finite element formulation have been supplied in the Section. Those may be plainly applied to the FE code in order to obtain the results of plane strain problems in the strain-gradient continuum mechanics.

6 Numerical examples

In this Section, some examples are solved in order to show the accuracy and validity of the elements developed in the current study. In all cases, the values of external loading are set in a way that not only the strains are small but also the magnitudes of the displacements are limited compared to the sides, so that the undeformed and deformed shapes are approximately equal. These considerations are the basis for the small deformation which is taken into account herein. All integrals in the current work are calculated using the Gaussian quadrature. In what follows, the superscripts C and SG refer to the classical and strain-gradient theories, respectively. Additionally, in all cases the depth of the body is ten times the largest side of a two-dimensional shape in the deformation plane in order to fulfill the plane strain situation. The point which must deemed herein is that generally the classical solution to the plane stress problems is more dominant than the plane strain ones, however as has been shown in [36], a plane strain response may be obtained from the corresponding plane stress solution by replacing E and ν with $E/(1-\nu^2)$ and $\nu/1-\nu$, respectively. Another important point which must be considered is that the PS12 is more accurate than PS6.

6.1 Uniaxial tension of a bar

In the current problem, extension of bar is dealt with. It is anticipated that the gradient effects are not active, since the deformation is homogenous [41]. Accordingly, it may be said that the strain-gradient and classical theories must have the same results. To examine the fact, let us study the deformation of a bar under extensional tractions at two ends, see Fig. 2. Taking account of the symmetry in the geometry and loading, one quarter of the whole region is modeled. Then, the symmetric boundary conditions at the central vertical line are

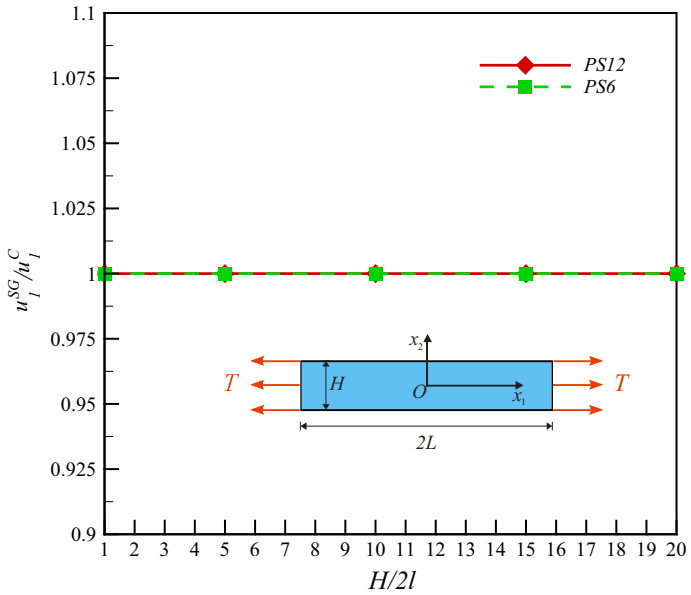

Fig. 2 The ratio of strain-gradient to classical predictions versus the various values of $H/2l$

$u_1 = \partial u_1/\partial x_2 = \partial^2 u_1/\partial x_2^2 = \partial u_2/\partial x_1 = \partial^2 u_2/\partial x_1 \partial x_2 = 0$, and the central horizontal line is $u_2 = \partial u_2/\partial x_1 = \partial^2 u_2/\partial x_1^2 = \partial u_1/\partial x_2 = \partial^2 u_1/\partial x_1 \partial x_2 = 0$. The classical solution to the problem is available to us as follows [36]:

$$u_1^{\mathrm{C}} = \frac{(1-\nu^2)T}{E} x_1 \tag{56}$$

where T is the applied traction.

Deem the length of the rectangle, $2L$, to be eight times the height, H, i.e., $2L = 8H$. The material properties of the body are supposed to be $E = 200$ GPa, $\nu = 0.3$, and $l = 0.1$ mm [42]. In addition, it is assumed that one half of the height of the solid is available in the various multiples of the material length scale l, i.e., $H/2 = nl$, so that the integer n varies from 1 to 20. To solve the problem using the finite element method, the geometry is discretized using 4×32 4-node plane strain elements. Also, Fig. 2 provides a comparison between the classical and strain-gradient solutions. In the Figure, the ratio of the strain-gradient and classical horizontal displacement of the tip is depicted versus the ratio of $H/2l$. The Figure indicates that the initial estimation was valid, as the strain-gradient and classical results have approximately the same results, the ratio u_1^{SG}/u_1^C is about one.

6.2 Cantilever beam under a transverse resultant

The second example is concerned with the flexure of a beam under a transverse loading, P, see Fig. 4. This was solved by Askes and Aifantis [29] and Fischer et al. [30] using the meshless method and isogeometric analysis, respectively. Following the references, for all cases analyzed herein the major assumption is that the length of the beam is thrice the height and the relation $H = nl$ holds where n changes from 1 to 20, see Fig. 4, and $E = 1000$ MPa, $\nu = 0.25$, and $l = 0.1$ mm. Following [29], the solutions to the problem are compared with the classical solution provided by Gere and Timoshenko [43]. Thus, the classical and strain-gradient stiffness read

$$k^{\mathrm{C}} = \frac{EH^3}{4L^3}, \qquad k^{\mathrm{SG}} = \frac{P}{\delta_{tip}}. \tag{57}$$

For this case, the whole geometry is divided into 8×24 4-node quadrilateral elements. Additionally, the boundary conditions at the constrained edge are

$$u_1 = \frac{\partial u_2}{\partial x_2} = \frac{\partial^2 u_2}{\partial x_2^2} = 0, \qquad u_2 = \frac{\partial u_2}{\partial x_1} = \frac{\partial u_2}{\partial x_2} = \frac{\partial^2 u_2}{\partial x_2^2} = \frac{\partial^2 u_2}{\partial x_1 \partial x_2} = 0. \tag{58}$$

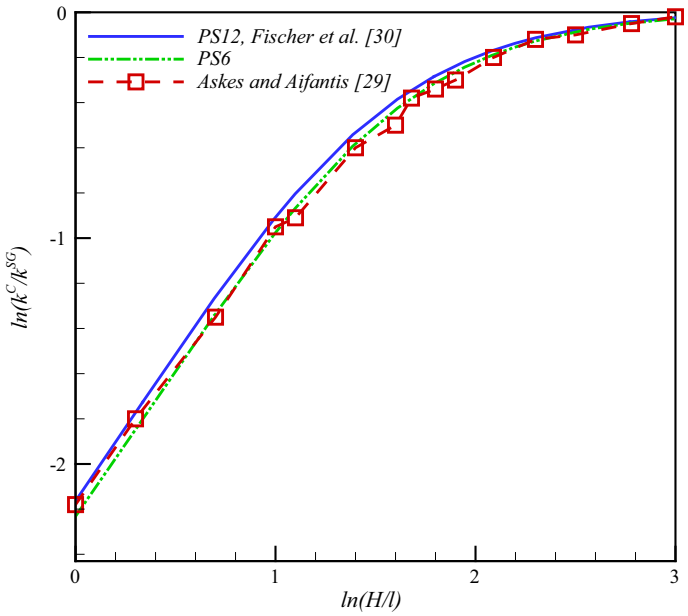

Fig. 3 The logarithm of the ratio of stiffness versus the logarithm of H/l

To compare the classical and strain-gradient solutions, Fig. 3 has been presented in which the natural logarithm of $k^{\mathrm{C}}/k^{\mathrm{SG}}$ is depicted versus the logarithm of H/l in the base of Napier's constant. As may be verified from the figure, for small values of H/l, say 1, the difference is significant, but for the large values of H/l, say 20, the distinction is indistinguishable. In addition, PS12 has the same result as the data reported by Fischer et al. [30], and the PS6 element provides an approximation.

The problem may be addressed in a different way given the classical response of the rectangle subjected to vertical end resultant in the plane strain deformation. The vertical deflection of the tip is $PL^3(1-\nu^2)/3EI$ [44]. It must be emphasized that the boundary condition used in the classical analysis is a little bit different from that used in the example due to Saint Venant approximation in loading; however, the classics provides us with an acceptable approximation. More precisely, the boundary condition just applies to the center of the constrained edge in the classics. As can be seen from Fig. 4, the curves regarding the central deflection of the tip normalized by the corresponding classical solution for various sizes have the same conclusion as Fig. 3.

6.3 Pure bending of a beam

The deformation of a beam under terminal resultant moments in the plane strain status is addressed in the current sample, see Fig. 5. To this end, H, $2L$, and M denote the thickness, length of the beam, and the applied external torque at the end given the Saint Venant principle. In addition, the geometric relations $H = nl$ and $L/H = 6$ are used in the analysis where n is a typical figure greater than one. Young's modulus, Poisson's ratio, and the material length scale parameter are $E = 200$ Gpa, $\nu = 0.3$, and $l = 0.1$ mm, respectively. Due to symmetry, just one half of the whole system is modeled using 8×48 finite elements. Additionally, the boundary conditions are as follows:

$$u_1 = \frac{\partial u_1}{\partial x_2} = \frac{\partial^2 u_1}{\partial x_2^2} = \frac{\partial u_2}{\partial x_1} = \frac{\partial^2 u_2}{\partial x_2 \partial x_1} = 0, \qquad x_1 = 0. \tag{59}$$

Besides, the vertical displacement of the center of the coordinate system $\{x_1, x_2\}$ is supposed to be zero in order to prevent the rigid-body motions.

From the textbooks in elasticity, the classical solution to the problem is available to us. Accordingly, the central vertical deflection reads [44]

$$u_2^{\mathrm{C}} = \frac{(1-\nu^2)ML^2}{2EI}. \tag{60}$$

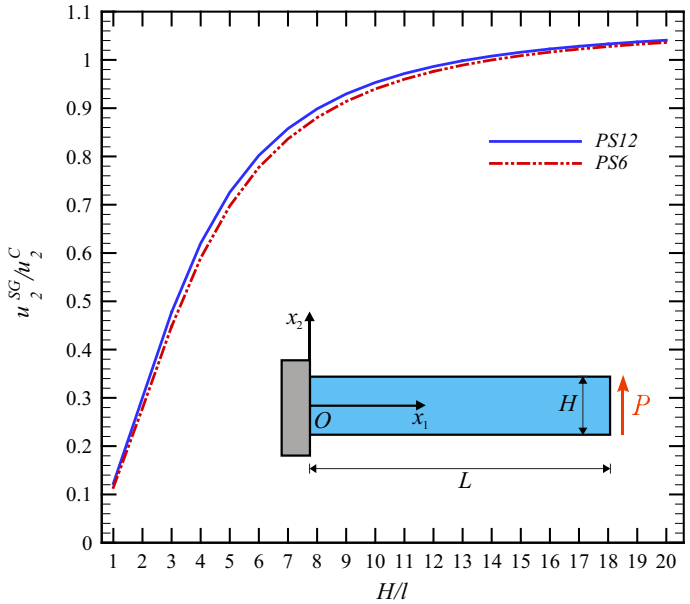

Fig. 4 Non-dimensional vertical deflection of the tip for various values of H/l

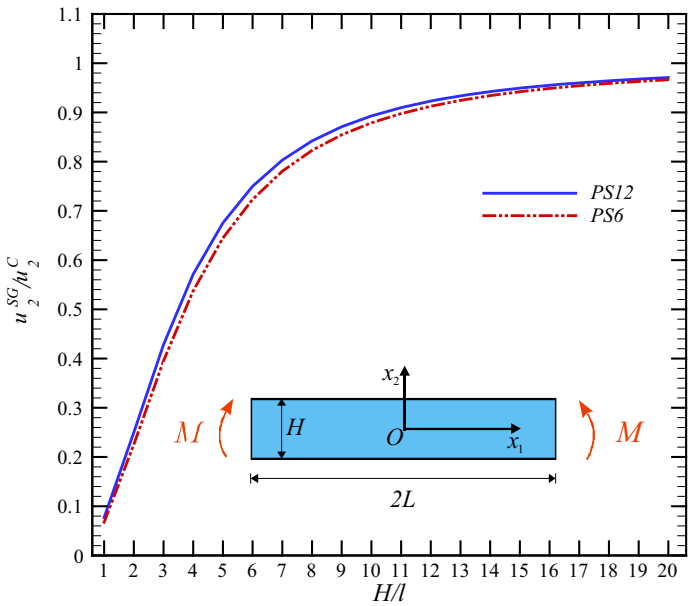

Fig. 5 Normalized deflection of the tip of the beam in different sizes

Figure 5 provides a comparison between the strain-gradient and classical responses for us. More precisely, in the Figure the non-dimensional parameter $u_2^{\mathrm{SG}}/u_2^{\mathrm{C}}$ for the end is depicted versus the parameter H/l. As may be verified from Fig. 5, by growing the ratio H/l, hence the size of the beam, the considerable difference between the strain-gradient and classical predictions reduces and finally disappears. In other words, the ratio of deflections changes from a value which is lower than 0.1 to approximately one.

6.4 Bending of a beam under distributed loading

The focus in the example is on the analysis of a beam which is simply supported at two ends, and a transverse uniform loading which is defined per unit length is imposed on the top surface as has been shown in Fig. 6.

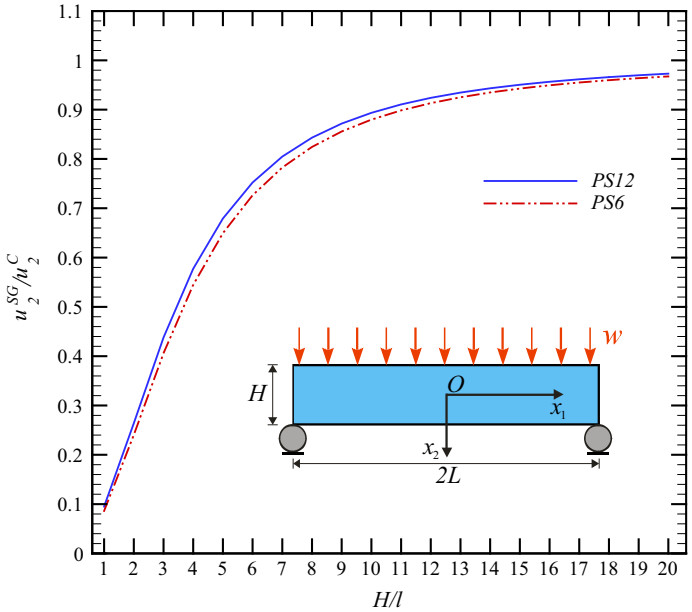

Fig. 6 The non-dimensional deflection versus the various values of H/l

Additionally, all geometric features have been included in the Figure. Also, it is assumed that the thickness is produced by multiplying the integer, n, and the material length scale parameter, l, and the half of the length, L, is five times the height, H. The material data are $E = 200$ Gpa, $\nu = 0.3$, and $l = 0.1$ mm.

Here, it is beneficial to take advantage of the symmetry condition which is $u_1 = \partial u_1/\partial x_2 = \partial^2 u_1/\partial x_2^2 = \partial u_2/\partial x_1 = \partial^2 u_2/\partial x_1 \partial x_2 = 0$ for $x_1 = 0$. Furthermore, the boundary conditions at the end read

$$u_2 = \partial u_2/\partial x_2 = \partial^2 u_2/\partial x_2^2 = 0, \qquad x_1 = L. \tag{61}$$

To continue analyzing the problem, it is worthy presenting the classical answer for the problem. What is of great importance to us is the maximum vertical deflection, hence it is

$$u_2^{\mathrm{C}}|_{\mathrm{MAX}} = \frac{5(1-\nu^2)wL^4}{24EI}\left[1 + \frac{3}{5}\left(\frac{4}{5} + \frac{\nu}{2(1-\nu)}\right)\frac{H^2}{L^2}\right] \tag{62}$$

for the classical mechanics [44].

To analyze the sample numerically, the number of elements in the horizontal and vertical axes for the half of the beam is 50 and 10, respectively, for producing square elements. Now, let us compare the strain-gradient and classical predictions. To this aim, Fig. 6 in which the parameter $u_2^{\mathrm{SG}}/u_2^{\mathrm{C}}$ for the origin is illustrated versus the parameter H/l has been presented. Clearly, increasing the size of the beam, i.e., H/l, diminishes the distinction between the strain-gradient and classical theories.

6.5 A thick hollow cylinder under pressure

The aim of this example is the investigation of the deformation of a hollow cylinder under the external pressure shown in Fig. 7. The effort for solving the problem numerically and analytically in the strain-gradient media was done by Zervos et al. [16]. To compare the current results which are on the basis of the conforming 4-node elements with the response obtained in [16], it is supposed that the radii of the internal and external circles are $R_1 = 0.05$ and $R_2 = 0.5$, respectively, and the material properties are $\lambda = 7000$, $\mu = 3000$, and $l = 0.01$. Due to the symmetry in the loading and geometry, only one quarter of the original model is modeled using 18×18 4-node elements. In addition, the following boundary conditions must be prescribed on the symmetry axes:

$$u_2 = \partial u_2/\partial x_1 = \partial^2 u_2/\partial x_1^2 = \partial u_1/\partial x_2 = \partial^2 u_1/\partial x_1 \partial x_2 = 0, \qquad x_2 = 0, \tag{63}$$

$$u_1 = \partial u_1/\partial x_2 = \partial^2 u_1/\partial x_2^2 = \partial u_2/\partial x_1 = \partial^2 u_2/\partial x_1 \partial x_2 = 0, \qquad x_1 = 0. \tag{64}$$

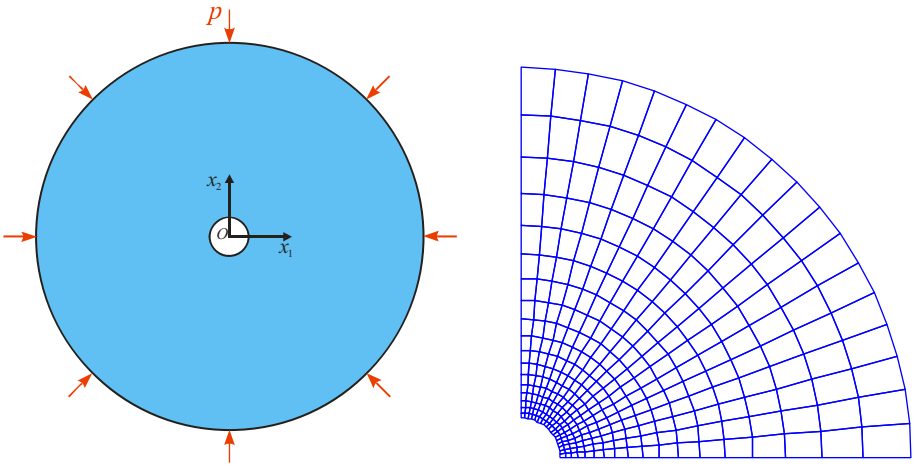

Fig. 7 The whole geometry and meshed region of the thick hollow cylinder

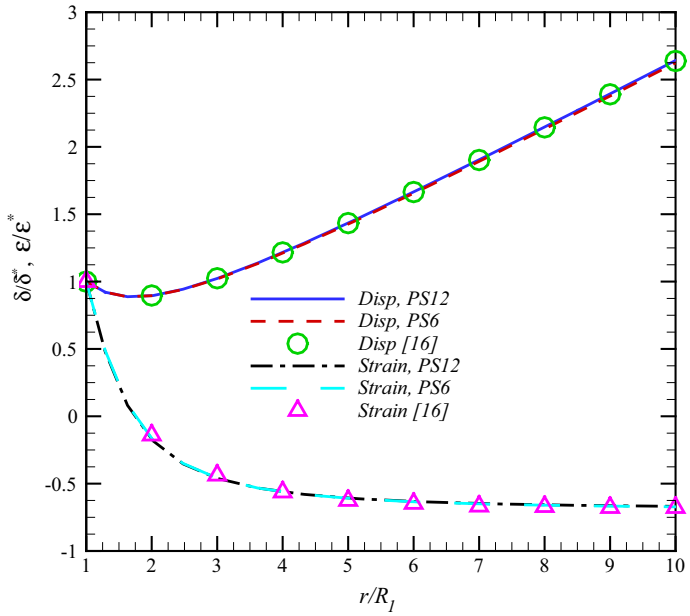

Fig. 8 Non-dimensional displacements and strains for points along the radius

The above boundary conditions are the direct results of an application of the symmetric deformed shape with respect to the axes x_1 and x_2. For more information on the application of the symmetric boundaries, Ref. [45] incorporates some invaluable data.

In addition, the non-dimensional displacement and strain along the radius which is normalized with respect to the quantities in the inner radius are shown in Fig. 8. As may be clearly seen from the Figure, there is a good agreement between current simulations and those reported in [16].

7 Conclusions

The conclusions and main focus of the current article can be listed as follows:

(i) The finite element analysis of the plane strain solids in strain-gradient elasticity was conducted in this work.

(ii) Following presenting the strains and strain-gradients in the plane deformation, the constitutive relations were used to find the corresponding stresses and double stresses.

(iii) Then, by applying the principle of virtual work, the weak form of the static stationary equation which is a key relation in FEM was obtained.
(iv) Due to presence of higher-order derivatives in the relations, higher-order DoF were included in the displacement vector. In such way, strain-gradient plane strain solid elements with 6 and 12 degrees of freedom per node were developed. Those are in the class of subparametric elements.
(v) Finally, some problems were analyzed to show the size-dependent behavior of solids in the small sizes, while in the large scale the difference is indistinguishable.

References

1. Aifantis, E.C.: Update on a class of gradient theories. Mech. Mater. **35**, 259–280 (2003)
2. Mindlin, R.D.: Micro-structure in linear elasticity. Arch. Ration. Mech. Anal. **16**, 51–78 (1964)
3. Mindlin, R.D., Eshel, N.N.: On first strain-gradient theories in linear elasticity. Int. J. Solids Struct. **48**, 109–124 (1968)
4. Aifantis, E.C.: On the role of gradients in the localization of deformation and fracture. Int. J. Eng. Sci. **30**, 1279–1299 (1992)
5. Kahrobaiyan, M.H., Asghari, M., Ahmadian, M.T.: A strain gradient Timoshenko beam element: application to MEMS. Acta Mech. **226**, 505–525 (2015)
6. Pegios, I.P., Papargyri-Beskou, S., Beskos, D.E.: Finite element static and stability analysis of gradient elastic beam structures. Acta Mech. **226**, 745–768 (2015)
7. Ru, C.Q., Aifantis, E.C.: A simple approach to solve boundary-value problems in gradient elasticity. Acta Mech. **101**, 59–68 (1993)
8. Chen, S.H., Feng, B.: Size effect in micro-scale cantilever beam bending. Acta Mech. **219**, 291–307 (2011)
9. Artan, R., Batra, R.C.: Free vibrations of a strain gradient beam by the method of initial values. Acta Mech. **223**, 2393–2409 (2012)
10. Lazopoulos, A.K.: Non-smooth bending and buckling of a strain gradient elastic beam with non-convex stored energy function. Acta Mech. **225**, 825–834 (2014)
11. Tsinopoulos, S.V., Polyzos, D., Beskos, D.E.: Static and dynamic BEM analysis of strain gradient elastic solids and structures. CMES **86**, 113–144 (2012)
12. Zienkiewicz, O.C., Taylor, R.L.: The Finite Element Method for Solids and Structural Mechanics, 6th edn. Butterworth-Heinemann, London (2005)
13. Akarapu, S., Zbib, H.M.: Numerical analysis of plane cracks in strain-gradient elastic materials. Int. J. Fract. **141**, 403–430 (2006)
14. Dasgupta, S., Sengupta, D.: A higher-order triangular plate bending element revisited. Int. J. Numer. Methods Eng. **30**, 419–430 (1990)
15. Papanicolopulos, S.A., Zervos, A., Vardoulakis, I.: A three-dimensional C1 finite element for gradient elasticity. Int. J. Numer. Methods Eng. **77**, 1396–1415 (2009)
16. Zervos, A., Papanicolopulos, S.A., Vardoulakis, I.: Two finite-element discretizations for gradient elasticity. J. Eng. Mech. **135**, 203–213 (2009)
17. Argyris, J.H., Fried, I., Scharpf, D.W.: The tuba family of plate elements for the matrix displacement method. Aeronaut. J. **72**, 701–709 (1968)
18. Petera, J., Pittman, J.: Isoparametric Hermite elements. Int. J. Numer. Methods Eng. **37**, 3489–3519 (1994)
19. Zervos, A.: Finite elements for elasticity with microstructure and gradient elasticity. Int. J. Numer. Methods Eng. **73**, 564–595 (2008)
20. Shu, J.Y., King, W.E., Fleck, N.A.: Finite elements for materials with strain gradients effects. Int. J. Numer. Methods Eng. **44**, 373–391 (1999)
21. Fleck, N.A., Hutchinson, J.W.: Strain gradient plasticity. Adv. Appl. Mech. **33**, 295–361 (1997)
22. Amanatidou, E., Aravas, N.: Mixed finite element formulations of strain-gradient elasticity problems. Comput. Methods Appl. Mech. Eng. **191**, 1723–1751 (2002)
23. Imatani, S., Hatada, K., Maugin, G.A.: Finite element analysis of crack problems for strain gradient material model. Philos. Mag. **85**, 4245–4256 (2005)
24. Askes, H., Gutiérrez, M.A.: Implicit gradient elasticity. Int. J. Numer. Methods Eng. **67**, 400–416 (2006)
25. Askes, H., Morata, I., Aifantis, E.C.: Finite element analysis with staggered gradient elasticity. Comput. Struct. **86**, 1266–1279 (2008)
26. Markolefas, S.I., Tsouvalas, D.A., Tsamasphyros, G.I.: Theoretical analysis of a class of mixed, C0 continuity formulations for general dipolar gradient elasticity boundary value problems. Int. J. Solids Struct. **44**, 546–572 (2007)
27. Markolefas, S.I., Tsouvalas, D.A., Tsamasphyros, G.I.: Some C0-continuous mixed formulations for general dipolar linear gradient elasticity boundary value problems and the associated energy theorems. Int. J. Solids Struct. **45**, 3255–3281 (2008)
28. Markolefas, S.I., Tsouvalas, D.A., Tsamasfyros, G.I.: Mixed finite element formulation for the general anti-plane shear problem, including mode III crack computations, in the framework of dipolar linear gradient elasticity. Comput. Mech. **43**, 715–730 (2009)
29. Askes, H., Aifantis, E.C.: Numerical modeling of size effects with gradient elasticity-formulation, meshless discretization and examples. Int. J. Fract. **17**, 347–358 (2002)
30. Fischer, P., Klassen, M., Mergheim, J., Steinmann, P., Müller, R.: Isogeometric analysis of 2D gradient elasticity. Comput. Mech. **47**, 325–334 (2011)
31. Tang, Z., Shen, S., Atluri, S.N.: Analysis of materials with strain-gradient effects: a meshless local Petrov–Galerkin (MLPG) approach, with nodal displacements only. CMES **4**, 177–196 (2003)

32. Tsepoura, K.G., Tsinopoulos, S., Polyzos, D., Beskos, D.E.: A boundary element method for solving 2-D and 3-D static gradient elastic problems. Part II: numerical implementation. Comput. Methods Appl. Mech. Eng. **192**, 2875–2907 (2003)
33. Bogner, F.K., Fox, R.L., Schmit, L.A.: The generation of interelement-compatible stiffness and mass matrices by the use of interpolation formulae. In: Proceedings of the 1st Conference on Matrix Methods in Structural Mechanics AFFDL-TR-66-80, pp. 397–443 (1966)
34. Lazar, M., Maugin, G.A.: Nonsingular stress and strain fields of dislocations and disclinations in first strain gradient elasticity. Int. J. Eng. Sci. **43**, 1157–1184 (2005)
35. Sokolnikoff, I.S.: Mathematical Theory of Elasticity. McGraw-Hill, New York (1956)
36. Sadd, M.H.: Elasticity: Theory, Applications, and Numerics. Academic Press, Oxford (2005)
37. Bathe, K.J.: Finite Element Procedures, 1st edn. Prentice-Hall, New Jersey (1996)
38. Zienkiewicz, O.C., Cheung, Y.K.: The finite element method for analysis of elastic isotropic and orthotropic slabs. Proc. Inst. Civ. Eng. **28**, 471–488 (1964)
39. Beheshti, A.: Large deformation analysis of strain-gradient elastic beams. Comput. Struct. **177**, 162–175 (2016)
40. Chandrupatla, T.R., Belegundu, A.D.: Introduction to Finite Elements in Engineering, 2nd edn. Prentice-Hall, Englewood Cliffs (1997)
41. Beheshti, A.: Generalization of strain-gradient theory to finite elastic deformation for isotropic materials. Contin. Mech. Thermodyn. **29**, 493–507 (2017)
42. Bagni, C., Askes, H., Susmel, L.: Gradient elasticity: a transformative stress analysis tool to design notched components against uniaxial/multiaxial high-cycle fatigue. Fatigue Fract. Eng. Mater. Struct. **39**, 1012–1029 (2016)
43. Gere, J.M., Timoshenko, S.P.: Mechanics of Materials, 3rd edn. Chapman & Hall, London (1991)
44. Timoshenko, S.P., Goodier, J.N.: Theory of Elasticity. McGraw-Hill, New York (1970)
45. Demkowicz, L.: A note on symmetry boundary conditions in finite element methods. Appl. Math. Lett. **4**, 27–30 (1991)